Journal Name

ARTICLE

# One-Pot Scalable Synthesis of All-Inorganic Perovskite Nanocrystals with Tunable Morphology, Composition and Photoluminescence

Received 00th January 20xx,
Accepted 00th January 20xx

DOI: 10.1039/x0xx00000x

www.rsc.org/

Emmanuel Acheampong Tsiwah[†a], Yanxi Ding[†a], Zixiong Li[a], Zhiyong Zhao[a], Mingqing Wang[b*], Chao Hu[a], Xiaoqing Liu[c], Chenghua Sun[d], Xiujian Zhao[a], Yi Xie[a*]

This study demonstrates a facile and general one-pot synthetic approach for all-inorganic colloidal cesium lead halide ($CsPbX_3$, X=Cl, Br, I, mixed Cl/Br, Br/I) perovskite nanocrystals (NCs) by directly heating the precursors/solvent/ligands. In contrast to typical routes, these reactions are conducted in open air, requiring neither high temperature dissolution nor vacuum/inert atmosphere. The composition, shape and size of the as-synthesized NCs can be finely tuned by varying the reaction parameters such as temperature and time, ligand species and precursor halide ratios. $CsPbX_3$ morphologies may be varied from perovskite nanoplatelets (NPLs) to nanosheets and sphere-like NCs, each with tunable absorption spectra and photoluminescence (PL) emissions. In particular, mixed halide NCs with controllable band gaps and PL emission across the entire visible region have been demonstrated by tuning the precursor halide ratios. The reproducibility and scalability of the present synthetic protocol is elaborated by up-scaling the amounts of chemicals and solvents/ligands in a representative synthesis of $CsPbBr_3$ NPLs. The representative large-scale $CsPbBr_3$ NPLs exhibit high PL quantum yield of 73.56%.

## Introduction

Historically colloidal metal chalcogenide nanocrystals (NCs) have been the most extensively explored family of efficient nanomaterials for photoluminescence (PL) applications nanomaterials for decades, more recent work has shown metal halide perovskites to be a promising alternatives.[1-24] In addition to hybrid organic-inorganic lead halides $APbX_3$ (A = $CH_3NH_3$/$NH_2CH{=}NH_2$, X = Cl, Br, I or mixed Cl/Br, Br/I), all-inorganic system such as cesium lead halide NCs ($CsPbX_3$) have emerged as one of the most interesting nanomaterials for optoelectronic applications due to their excellent optical properties, such as size- and composition-dependent emission wavelengths, emission with a narrow full-width at half-maximum (FWHM), and high luminescent efficiency.[1, 3, 5, 9, 13, 25-31]

Like other semiconductors, the morphology, size and composition of perovskite NCs could be manipulated to tune the optical properties including band-band absorption spectra and PL emission over the entire visible spectral range.[1, 16, 32-35] Compositional control in perovskite NCs was usually achieved by post-synthetic halide exchange in the as-synthesized single-halide NCs.[1, 16, 36] Size tunability in perovskite NCs with various morphologies (e.g. nanocubes, nanoplatelets (NPLs), nanosheets, nanorods and nanowires) was recently reported in a direct synthesis reaction by several groups.[2, 26, 28, 37-47] Size and morphology control could be accomplished by tailoring the reaction parameters such as temperature[48] and ligand mediation.[38, 44, 49] $CsPbX_3$ NCs are most commonly created using hot-injection methods,[1, 5, 10, 28, 36, 50, 51] however, recently non-hot-injection such as heat-up and room temperature (RT) routes have been developed.[2, 15, 43, 52] have been devoted to the generation of various colloidal $CsPbX_3$ NCs. Kovalenko et al. successfully synthesized monodisperse $CsPbX_3$ nanocubes,[48] which involved a rapid injection of Cs precursors (e.g. Cs-oleate) into the lead halide precursors being pre-dissolved in oleylamine (OM), oleic acid (OA) and octadecene (ODE) at high temperature (e.g. 165 $^oC$).

To realize the commercial application of NCs, synthetic approaches must produce high-quality all-inorganic $CsPbX_3$ NCs in a scalable, reproducible and inexpensive manner, while enabling the high-yield production. The widely studied hot-injection procedure, involving the injection of precursors into hot reaction media under inert gas protection, is unsuitable for large-scale generation of perovskite NCs. Alternatively, other techniques such as heat-up and RT reaction involving a single one-pot setup at RT, can be readily extended to the gram-scale level,[53-55] and have been shown compatible with perovskite NCs production.[2, 15, 43, 52] Akkerman et al. reported the RT synthesis of $CsPbBr_3$ NPLs in open air by mixing Cs-oleate precursor, HBr and $PbBr_2$ precursors, in which Cs-oleate was prepared by dissolving $Cs_2CO_3$ in ODE and OA at 150 °C.[2] However, currently most reported heat-up or RT approaches involve either the pre-dissolving Cs and/or Pb precursors at high temperature before mixing or the introduction of a toxic solvent such as dimethyl formamide (DMF).[2, 15, 42, 52]

[a] *State Key Laboratory of Silicate Materials for Architectures, Wuhan University of Technology (WUT), No. 122, Luoshi Road, Wuhan 430070, P. R. China. E-mail: xiey@whut.edu.cn; Tel.: +86-15527835639.*
[b] *UCL Institute for Materials Discovery, University College of London, Room 107, Roberts Building, Malet Place, London WC1E 7JE, United Kingdom. E-mail:* mingqing.wang@ucl.ac.uk.
[c] *Center of Materials Research & Testing, Wuhan University of Technology, Wuhan, Hubei 430070, P.R. China.*
[d] Department of Chemistry and Biotechnology, Faculty of Science, Engineering & Technology, Swinburne University of Technology, Hawthorn, VIC 3122, Australia.
† These authors contributed equally to this work.
Electronic Supplementary Information (ESI) available: Additional TEM/HRTEM images, XRD patterns, PLQY, optical spectra, photographs of NC dispersions under normal indoor light and UV illumination, size distribution histograms. See DOI: 10.1039/x0xx00000x

We are thus motivated to explore a facile one-pot NCs synthesis, which involves directly heating the mixture of all precursors/solvent/ligands to the desired temperature for reaction. Toward this goal, $CsPbX_3$ NCs with controllable morphology (Scheme 1), size, composition and optical properties have been created. Here the route is demonstrated in open air, without vacuum/inert environment, wherein the size, shape, composition, absorption band and PL emission spectra can be easily controlled. . We finally demonstrate the advantages of the present one-pot route in the reproducibility and scalability of perovskite NCs.

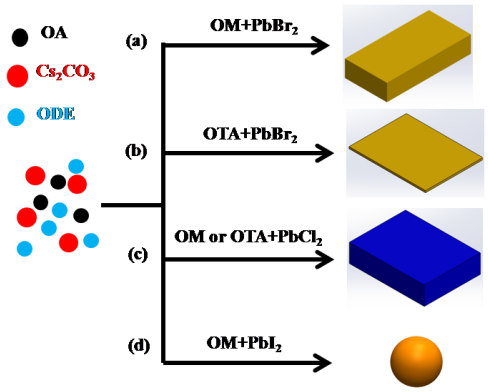


**Scheme 1.** One-pot synthetic route to various $CsPbX_3$ (X = Cl, Br, I) NCs with tunable morphologies.

## Experimental

### Chemicals and Materials

Lead(II) chloride ($PbCl_2$, 99.999% trace metals basis), lead(II) bromide ($PbBr_2$, 99.999% trace metals basis), lead(II) iodide ($PbI_2$, 99.999% trace metals basis), octylamine (OTA, 99.0%) cesium carbonate ($Cs_2CO_3$, 99%) were purchased from Sigma-Aldrich, octadecene (ODE, technical grade, 90%) and oleylamine (OM, 80-90%) from Aladdin, oleic acid (OA, 90%) and hexane from Macklin. All chemicals were used as received without any further purification.

### $CsPbX_3$ (X = Cl, Br, I, Cl/Br, Br/I) NCs Synthesis

The synthesis of all the $CsPbX_3$ NCs were performed in open air.. In a typical synthesis of $CsPbBr_3$ NPLs, a mixture of $PbBr_2$ (69 mg, 0.188 mmol) and $Cs_2CO_3$ (11 mg, 0.033 mmol) was loaded in a 50 mL three-neck flask containingODE (10 mL), OA (0.5 mL) and OM (1.0 mL). The mixture was stirred at RT for 20 min before heating to 110 °C at1 °C/min and holding at 110 °C for 10 min. During heating, metal salts gradually dissolved and translucent solution formed at 55-70 °C. The resulting yellow dispersion was cooled down to RT, and the synthesized nanoparticles (NPs) were directly collected via high speed centrifugation (at 10,000 rpm for 15 min) and finally suspended in 1 mL hexane for further characterizations. Perovskite $CsPbBr_3$ nanosheets were synthesized through the same procedure, by replacing ligand OM with OTA. The generation of $CsPbCl_3$, $CsPbI_3$ and mixed halide NCs were conducted through the same protocol by replacing $PbBr_2$ with $PbCl_2$ (52mg), $PbI_2$ (87 mg) or mixed halide precursors (i.e. $PbCl_2$/$PbBr_2$ and $PbI_2$/$PbBr_2$), respectively.

### Scalability and Reproducibility of NCs Synthesis

The procedure of the large-scale synthesis is the same as described above, except that 10-fold amounts of precursors/ligands/solvent were used in the reaction. Typically, 0.690 g of $PbBr_2$ and 0.110 g of $Cs_2CO_3$ were loaded in a 1000-mL three-necked flask containing 5 mL OA, 10 mL of OM and 100 mL of ODE, followed by heating up to 110 °C and keeping the reaction at 110 °C for 10 min. The resulting dispersion was cooled down to RT, and the NCs were cleaned by high speed centrifugation (at 10000 rpm for 15 min) and finally dispersed in hexane for further characterization.

### Transmission Electron Microscopy (TEM)

Conventional TEM and high-resolution TEM (HRTEM) images were acquired on a JEM 2100F (JEOL, Japan) microscope equipped with a field emission gun working at 200 kV accelerating voltage. The samples were prepared by drop-casting nanocrystal (NC) solutions on 300 mesh Cu grids covered with ultrathin amorphous carbon film, which were then placed in a high vacuum pumping station in order to let the solvent completely evaporate and preserve the NCs from oxidation.

### X-ray Diffraction (XRD)

The phase attribution and lattice parameter were analyzed by testing film of the as-synthesized NCs on a Bruker D8 Advanced X-ray diffractometer equipped with a 1.8 kW CuKα ceramic X-ray tube, operating at 40 kV and 40 mA. The XRD patterns were collected in air at RT in Bragg-Brentano parafocusing geometry with a step size of 0.02°. All XRD film samples were prepared by drop-casting a concentrated NC solution on a glass wafer. The data analysis was carried out using X'PertHighscore plus software from PANalytical.

### Optical Absorption Spectroscopy

The optical absorption spectra of the NC solutions were collected with a UV-3600 UV-Vis-NIR spectrophotometer (Shimadzu, Japan) in the 300-900 nm wavelength range. Sample preparation was performed inside a $N_2$-filled glove box, by using hexane as solvent. The diluted NC solutions were prepared in 1 cm path length quartz cuvette with airtight screw caps.

### Steady-State PL Measurements

The sample preparation was identical to that in the above-mentioned optical absorption test. The steady-state PL measurements were collected by exciting the samples at 355 nm, which were recorded with a 355 laser source modulated by mechanic chopper and a combination of monochromator, photomultiplier detector, and lock in amplifier (MPL-F-355-100 mW 13120588, Changchun New Industries Optoelectronics Tech. Co. Ltd, China). For comparison, the results were normalized at the maximum intensity of the PL emission peak.

### Time-Resolved PL and PL Quantum Yield (PLQY) Measurements

Time-resolved PL measurement of the representative large-scale $CsPbBr_3$ NCs was acquired using a phosphorescence lifetime spectrometer (Edinburgh, FLS 980) equipped with a 375 nm, 60.8 ps pulse width laser and a time-correlated single-photon counting setup at room temperature. The PLQY of $CsPbX_3$ NCs was calculated according to the method described by Manna and coworkers.[1] PL spectra for PLQY measurement and calculation were recorded using the same Edinburgh equipment (FLS 980), by exciting the diluted NC colloidal sample with 400 nm. The exciting light was coupled to an optical fiber connected to an integrating sphere in which a quartz cuvette with NC solution was placed. Four data were collected for the calculation: the sample emission (SEM), the sample excitation (SEX), the blank emission (BEM), and the blank excitation (BEX), based on which the PLQY was estimated as

$$\mathrm{PLQY}(\%) = \frac{\mathrm{SEM} - \mathrm{BEM}}{\mathrm{BEX} - \mathrm{SEX}} \times 100$$

**Thermo Gravimetric Analysis (TGA)**

The measurement of mass changes and thermal effects between 25 °C to 450 °C was carried out using Simultaneous Thermal Analyzer (STA 449 F3 Jupiter). Powder sample of perovskite NC was used for analysis TG-DSC under Ar atmosphere.

## Results and discussion

**One-Pot Synthesis of $CsPbBr_3$ NCs with Tunable Morphological and Optical Properties**

In order to understand better the reaction mechanism, we tried first of all the typical reactions in the presence of OA, OM and OTA alone. ODE serves as a non-coordinating solvent, while OM, OA and OTA may act as ligands and play critical roles in the tunable synthesis. The metal salt precursors did not fully dissolve (and no NCs were produced) in the presence of OA alone (i.e. no OM and OTA), indicating that amine is essential for all the syntheses discussed herein. Conversely, OA was required for all syntheses involving iodides. OTA alone in the reaction led to the generating only Br- and Cl-based NCs with PL emission, and OM alone resulted in the formation of only Br-based NCs, (Figure S1 of the Supporting Information, SI). The above samples are not uniform in size and shape (Figure S1c-e of the SI).

The presence of both OA and amine (OM or OTA) allows fine control over the synthesis; the morphological, structural and optical properties were measured throughout the reaction (Figure 1a-b, d-e, g-h, more details in Figures S2-5 of the SI).. Compared with the previously reported high-temperature hot-injection protocol involving evacuation process and inert atmosphere, the current approach confirms the generation of Cs-Pb-Br NCs through a general facile route of cooking the precursors/solvent/ligands at modest temperatures in open air. The reaction at 90-100 °C led to the formation of nanocubes (Figure 1a, Figure S2a-b of the SI), however, further heating led to the as-formed nanocubes converting to NPLs (Figure 1b, Figure S2c-e of the SI). The average size of NCs calculated from TEM images increased from 5.3 ± 0.5 nm of the nanocubes ((i.e. the cube edge length) to 7.0 nm in thickness of the NPLs (Figure S4, Table S1 of the SI). Higher temperatures (>165 °C) led to heavy agglomeration of the NCs (Figure S2f of the SI). Two distinct phases of $CsPbBr_3$ and $Cs_4PbBr_6$ are detected from the XRD patterns of the as-synthesized nanocubes (Figure 1g, Figure S3c of the SI). It was noticed that the attribution of XRD patterns needs scrutiny due to the small differences among perovskite $CsPbBr_3$.[45] We therefore provide the representative orthorhombic (JCPDS No. 98-009-7851) and cubic (JCPDS No. 00-054-0752) phases for comparison (Figure S3c of the SI). The experimental peaks of the various samples at two theta of ~15.2°, 21.4°, 24.1°, 25.4°, 26.4°, 28.6°, 30.4°, 30.7° and 37.7°, 43.7° are tentatively assigned to orthorhombic $CsPbBr_3$ (JCPDS No. 98-009-7851). The diffraction peaks observed at 12.7°, 22.5°, 27.5°, 28.6° and 39.9° in the nanocubes are indexed to (012), (300), (131), (214) and (324) planes of rhombohedral $Cs_4PbBr_6$ ((JCPDS No. 01-073-2478, Figure 1g). At increasing temperature, the XRD peaks of synthesized samples are in complete agreement with the standard orthorhombic crystal structure of perovskite $CsPbBr_3$ (Figure 1g, black curve, and Figure S3c of the SI), indicating that the rhombohedral $Cs_4PbBr_6$ nanocubes converted to orthorhombic $CsPbBr_3$ NPLs upon heating. The structural conversion can be further evidenced by HRTEM analysis on the single NCs (Figure 1d-e, Figure S5a-d of the SI). The lattice spacing of 0.396 nm corresponds to the (300) plane of the rhombohedral $Cs_4PbBr_6$ phase (Figure 1d, Figure S5a-b of the SI), while the characteristic lattice spacing of 0.412 and 0.290 nm can be respectively assigned to the (200) and (202) planes of the orthorhombic $CsPbBr_3$ structure (Figure 1e, Figure S5c-d of the SI). Despite the difference of phase and morphology, both the nanocubes and NPLs display green emission (Figure 1h), visibly observable in the NC solution (in hexane) under UV light (inset of Figure 1a-b). The increase in size from nanocubes to NPLs explains the redshifted band-band absorption peaks and PL emission bands from 482.8 to 502.0 nm and 492.0 to 525.0 nm, respectively (Figure 1h, Figures S2-4 and Table S1 of the SI), due to the quantum confinement in the as-formed NCs.[48] The representative bromide NCs are featured by narrow emission bands at around 492-512.9 nm with FWHM of 18.2--26.0 nm (Table S1 of the SI).

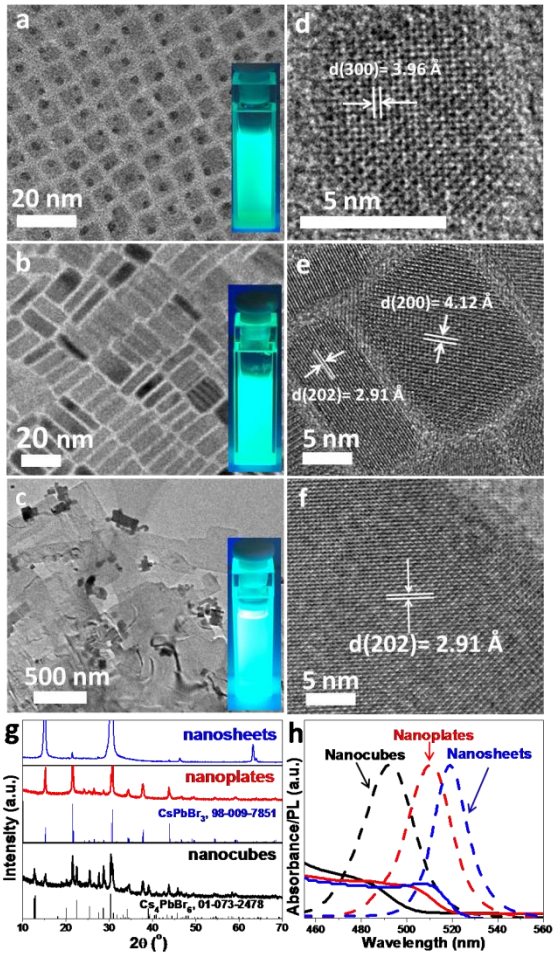


**Figure 1.** (a-f) Representative TEM (a-c) and HRTEM images (d-f) of Cs-Pb-Br nanocubes (a, d), $CsPbBr_3$ NPLs (b, e) and nanosheets (c,f), respectively. (g-h) Experimental XRD patterns along with the standard XRD patterns of orthorhombic $CsPbBr_3$ (JCPDS No. 98-009-7851) and rhombohedral $Cs_4PbBr_6$ (JCPDS No. 01-073-2478) (g), optical spectra (solid curves) and PL emission bands (dashed curves) (h) of the corresponding NCs. Insets in panels a-c) present the photographs of corresponding NC solution (in hexane) under UV light illumination (355 nm excitation wavelength).

The morphological transformation from nanocubes to NPLs can also be realized by prolonging reaction time at fixed temperature (e.g. 95 °C), as evidenced by the TEM images (Figure S6a-d of the SI). The average cube edge length increases from an initial 5.7 nm to 7.0 nm at 30 min (Table S2 of the SI). As the reaction proceeds, plate-like NCs with average thickness of 7.3 nm, and lateral sizes of 24 nm and 15

nm, respectively, are generated at 60 min (Figure S6c and Table S2 of the SI). The XRD patterns display the presence of mixed phases of orthorhombic $CsPbBr_3$ and rhombohedral $Cs_4PbBr_6$ in the nanocubes (Figure S6e of the SI), as seen for the heated experiments. However, increasing reaction time *in* lieu of temperature leads to a significant increase in the proportion of orthorhombic phase. The UV-Vis optical spectra of the as-synthesized NCs exhibit single band-band absorption peak and PL emission (Figure S6f-g of the SI). The absorption edge and PL emission peaks are gradually redshifted respectively from ~515.2 to 527.2 nm and from ~504.9 to 519.0 nm, with increasing reaction time (Figure S6f-g of the SI). Overall by tailoring the time and temperature, the narrow FWHM is identified as 18.2-26.0 nm in the Br-based NCs (Tables S1-S2 of the SI). The absorption spectra and PL emission of bromide NCs in our work are similar to previously reported all-inorganic Br-based perovskite NCs of comparable size.[1, 48, 56, 57]

Tailoring the ligand ratio or ligand species has been reported to be an effective way to control shape/size of perovskite NCs and thus to tune the excitonic absorption and PL emission.[34, 44, 58] The reaction of $PbBr_2$ ($PbCl_2$ and $PbI_2$, , *vide supra*) with $Cs_2CO_3$ in the presence of OA alone failed to form NCs; the introduction of amine is essential in the synthesis. During synthesis, the metal salt precursors gradually dissolved to give translucent solution at around 55-70 °C, dependant on the specific precursors/ligands. It can thus be rationalized that intermediary complexes form at some point of the reaction due to the coordinating cations (e.g. $Pb^{2+}$) by capping ligands.[59] Further increasing temperature triggers the formation of nuclei,[59] and finally leads to the growth of nuclei into NCs. On the basis of these considerations, the effect of OM quantity and ligand species (e.g. OTA) on the synthesis was investigated. In contrast to previous reports of shape/size tunability ,[44] here changing the OM concentration displayed no noticeable effects on the phase, shape, size or optical properties of the resulting perovskite $CsPbBr_3$ NCs (Figure S7 of the SI). Interestingly, by replacingOM with OTA, rectangle-shaped nanosheets of micrometers scale lateral sizes formed, as seen in TEM observation (Figure 1c, Figure S8b-c of the SI). The change in shape is attributed tothe preferential binding of ligand to specific crystal facets, allowing for different anisotropic growth rates for different crystal planes.[44] The generation of $CsPbBr_3$ NCs in the presence of OTA required higher temperature (e.g. 130 °C) compared with OM; reactions at temperatures below 100 °C generated no NCs. Temperature of 110-120 °C led to the formation of irregularly-shaped NPs (Figure S8a and S10a-b of the SI). XRD analysis showed these NPs contained mixed phases of $Cs_4PbBr_6$ and $CsPbBr_3$ (Figure S8h of the SI). Increasing the reaction temperature or time allowed for the generation of nanosheets in the perovskite $CsPbBr_3$ phase, as confirmed by both XRD and HRTEM analyses (Figure 1f-g). Both absorption edge and PL emission band of the high temperature nanosheets were slightly redshifted compared to the relatively low temperature ones (Figures S8f-g of the SI), likely due to the increment of particle size in thickness. With further increasing temperature or reaction time, the nanosheets underwent partial etching, becoming irregular in shape, and forming holes (Figures S8d-e and S10c-d).

**One-Pot Synthesis of Chloride, Iodide and Mixed Halide NCs with Tunable Morphological and Optical Properties**

It is noteworthy that the present one-pot synthetic approach is appealing to not only perovskite NCs of bromides but also to chlorides, iodides and mixed halides with wider colour emissions. By simply replacing $PbBr_2$ with $PbCl_2$ during the synthesis, $CsPbCl_3$ NCs are formed. A typical reaction at 95 °C for 30 min forms square-shaped NPLs with average lateral edge length of ~40 nm and thickness of ~4.6 nm. (Figure 2a, Figure S11 of the SI). By analogy with the bromide synthesis, the NCs formed at the early synthetic stage in the reaction contained mixed phases including cubic $CsPbCl_3$ phase (JCPDS No. 98-020-1250) and monoclinic $Cs_4PbCl_6$ phase (JCPDS No. 01-078-1685) (Figure S12a of the SI). As the reaction proceeded, the representative NPLs were identified by XRD and HRTEM to be in only cubic $CsPbCl_3$ phase (Figure 2d, g andFigure S12a of the SI). Akin to $CsPbBr_3$, the optical absorption edge exhibited slight red-shift with increasing reaction time (Figures S12b-c of the SI), reflective of the increase in NPL size. In addition, increasing the fraction of OM (relative to OA) in the reaction system resulted in slight shift of PL emission band but no noticeable change of morphology can be observed (Figure S13 of the SI).

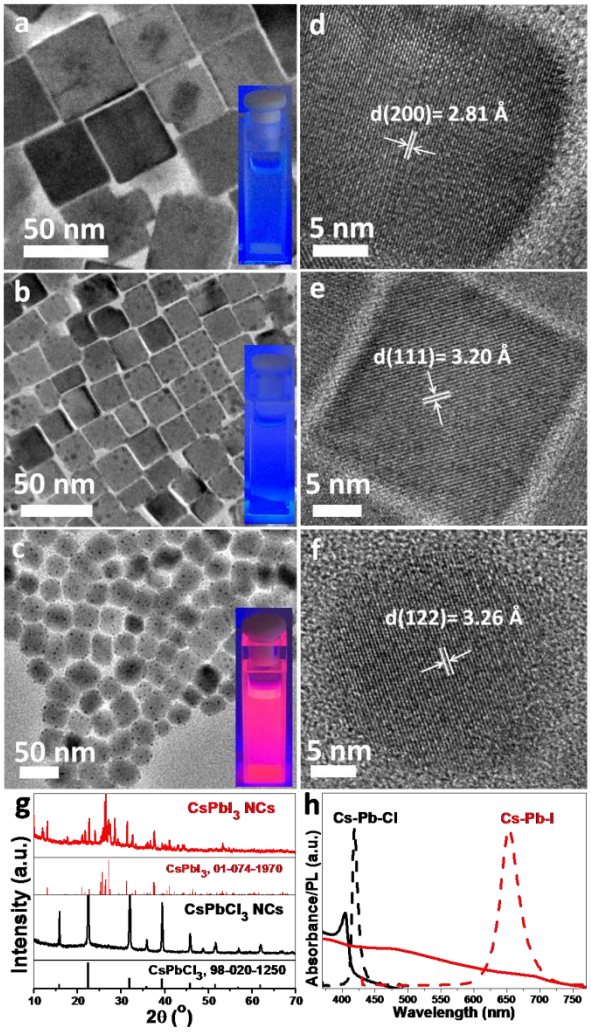


**Figure 2.** (a-f) TEM (a-c) and HRTEM images (d-f) of the representative perovskite $CsPbCl_3$ NCs as-synthesized in the presence of OA and OM (a, d), OA and OTA (b, e), respectively, and $CsPbI_3$ NCs collected in the presence of OA and OM (c, f). (g-h) XRD patterns (g), absorption spectra (solid line) and PL band (dashed line) (h) of the corresponding NCs in panels a) and c), respectively. Insets in panels a-c) display the photographs of the corresponding NC solution (in hexane) under UV light illumination (355 nm excitation wavelength).

The generation of Cl-based NCs in the presence of OA and OM occurs at 95 °C, however, higher reaction temperatures (e.g. over 110 °C) were required when OM was used in lieu of OTA, analogous to the Br-based NC synthesis. Temperatures below 130 °C led to the generation of mixed phases of cubic $CsPbCl_3$ and monoclinic $Cs_4PbCl_6$ (Figure S15a of the SI). Increasing reaction temperature and time allowed for the formation of cubic $CsPbCl_3$ (JCPDS No. 98-020-1250), in line with the temperature-dependent evolution in the presence of OM. Typically, the $CsPbCl_3$ NPLs collected at 130 °C displayed average lateral edge lengths of ~22.1 and thickness of ~3.2 nm (Figure 2b, Figure S16a of the SI). Similarly, red-shift of absorbance spectra and PL emission band were observed with increasing reaction temperature and time (Figures S15b-c and S17e-f of the SI). Overall the PL band can be tuned from 411.0 to 419.1 nm, depending on the specified reaction parameters in the synthesis.

Additionally, the synthesis of iodine-based NCs was also investigated, however, several differences from the bromide and chloride NCs were evident (additional details can be found in Figures S18-20 of the SI). Firstly, no any NCs were formed using OTA as the capping amine, even when increasing the temperature to 180 °C. Secondly, the morphology and particle size were more sensitive to both temperature and time. At the early stage in the reaction (i.e. 0 min at 95 °C), sphere-like and rhombus-like NPs were formed (Figure 2c). At the later stage (e.g. 5-20 min), rod-like particles emerged (Figure S18b-c of the SI). With longer time or higher temperature (e.g. above 110 °C), large rods with average length of ~2.0 µm and thickness of ~200 nm dominated the product (Figure S18d-e of the SI). The phase of the sphere-like NPs can be assigned to orthorhombic $CsPbI_3$ (JCPDS No. 00-018-0376) although diffraction peaks at two theta of ~12.1°, 17.7°, 24.1° and 28.5° remain unassigned and are attributed to impurities (Figure 2g, red curve). Notably, these minor diffraction peaks vanished after 20 min of the reaction, and peaks of orthorhombic phase are completely predominant in the samples (Figure S19a of the SI), which are similar to previously-reported $CsPbI_3$ nanowires.[45] HRTEM images of the representative tip of single rod exhibited lattice spacing of 0.329 nm, corresponding to the (122) plane of orthorhombic $CsPbI_3$ (Figure S20 of the SI). Red emission ranging 653.0-694.0 nm can be observed in the NCs collected within 20 min (Figure S19c of the SI). However, the rod-like particles displayed no PL band due to their large size.

In the various perovskite NCs, high-contrast dots were observed on some of TEM images (e.g. Figures 1a, 2b-c, and Figures S6a-c, S17a of the SI), in which some of the NCs displayed dimer-like feature. This effect is known to occur due to the radiolysis of the as-formed $CsPbX_3$ NCs and subsequent formation of metallic Pb upon E-beam irradiation.[2, 37, 60] The systematic elucidation on the morphological and compositional evolution of the $CsPbBr_3$ NCs has shown that E-beam irradiation led to the desorption of Br atoms from the initial NCs and the reduction of $Pb^{2+}$ ions to $Pb^0$.[61] Indeed, by prolonging the E-beam irradiation time, additional high-contrast particles emerged and finally some of the initial NPs were destroyed (Figure S21 of the SI).

As elucidated above, the PL bands of each single halide NCs could be tuned by tailoring the particle shape and size. Overall the PL emission bands of single chloride, bromide and iodine NCs can be tuned at around 415 nm, 510 nm and 680 nm, respectively. In order to realize a continuum of $CsPbX_3$ materials across the entire visible spectrum, mixed halides NCs were investigated using different halides of varied ratios (i.e. mixed precursors of $PbCl_2$ and $PbBr_2$, or mixed $PbBr_2$ and $PbI_2$). The TEM micrographs and UV-Vis optical spectra (Figure 3) demonstrate successful formation of coherent NCs. Precisely adjusting halide ratios in the precursors allowed a range of amterials with well-tuned PL emission bands covering the visible spectral range from 417 to 688 nm (see also Figures S22-23, and Tables S3-4 of the SI). Both the band-band absorption features and the PL emission peak can be finely tuned to a longer wavelength region with increasing either precursor Br:Cl ratio in the Br/Cl-mixed NCs or precursor I:Br ratio in the case of Br/I-mixed ones. Furthermore, narrow emission band with FWHM ranging from 10.6 to 45.8 nm were achieved in the synthesized mixed halide NCs (Tables S3-4 of the SI).

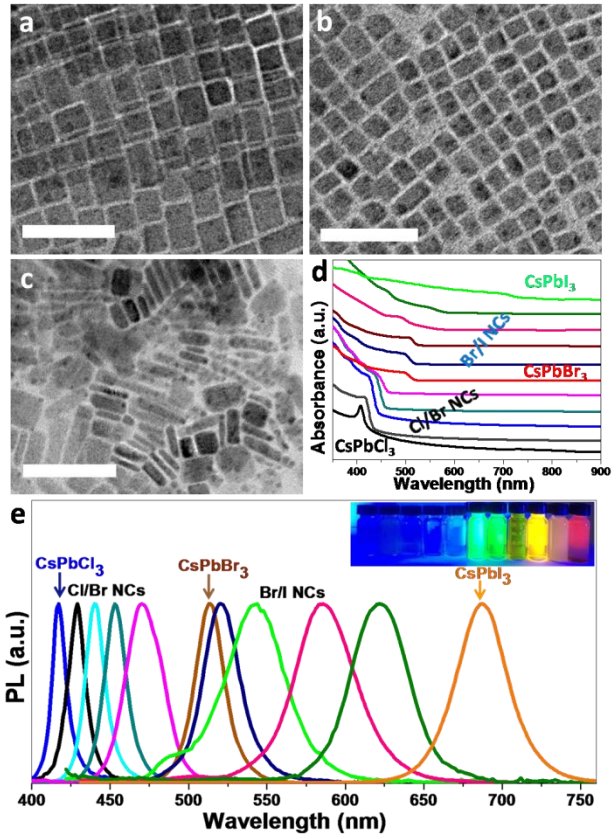


**Figure 3.** Characterization of single halide perovskite (i.e. $CsPbCl_3$ and $CsPbBr_3$) and mixed halides NCs (i.e. $CsPbBr_{3-x}Cl_x$) prepared via a one-pot synthetic approach by tuning the precursor halide ratios. (a-c) TEM images of mixed halide NCs synthesized with starting Cl:Br ratio of 2:1 (a), Br:I ratio of 2:1 (b) and 1:4 (c), respectively. The scale bars are 50 nm. (d-e) absorption spectra (d) and PL emission bands (e) of the single halides and mixed halide NCs. Inset in panel e) provides the photograph of the various NC solutions (in hexane) under UV light illumination.

**Scalability and Reproducibility of the One-pot Synthetic Approach**

The present one-pot facile approach requires no special equipment and thus readily extends to large-scale generation – as a demonstrator, a scaling of $CsPbBr_3$ by an order of magnitude was performed (Figure 4a). The TEM image displayed the presence of monodisperse NPLs with average lateral sizes of 21 and 15 nm, and average thickness of 7.0 nm, respectively ( Figure S24d of the SI). XRD analysis (Figure 4b) confirmed the formation of orthorhombic perovskite $CsPbBr_3$ (JCPDS No. 98-009-7851). This can be further verified by HRTEM analysis (Figure S24e of the SI), which revealed a crystalline feature of the single NCs with lattice spacing of 0.290 nm, corresponding the (002) plane of orthorhombic structure. UV-Vis optical spectra together with a photograph of NC solution in hexane

(Figure 4c) displayed bright green emission (355 nm excitation wavelength) with narrow emission line-width of ~21 nm. By fitting the time-resolved PL with a triexponential decay function (Figure 4d, Figure S24h of the SI), an average PL decay lifetime of 7.76 ns was derived. This is comparable to the decay lifetime of $CsPbBr_3$ NCs previously reported.[2, 48] The percent yield of the perovskite NCs, estimated based on the comparison of the actual yield and the theoretical yield, where the ligand weight calculated from TGA analysis was subtracted (Figure S24g of the SI), was 64.52%. The large-scale $CsPbBr_3$ NPLs exhibited PLQY of 73.56%, which is comparable with those of previously reported Br-based perovskite NCs.[1, 2] These features are in good agreement with those in small-scale synthesis, and thus conclusively demonstrate that the present synthetic procedure can be scalable and reproducible, rendering it a desirable general protocol for NC engineering.

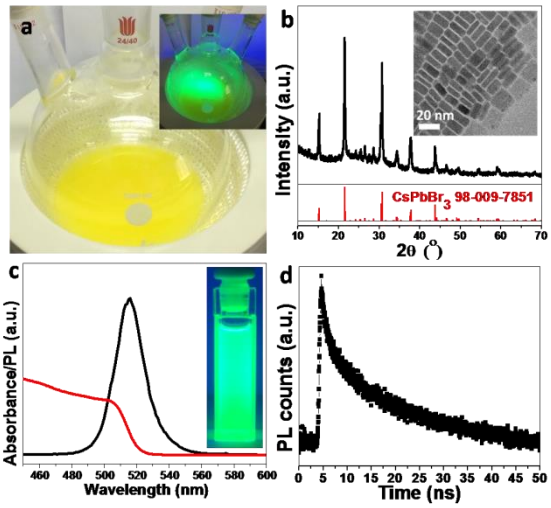


**Figure 4.** Characterization results of perovskite $CsPbBr_3$ NCs obtained via large-scale synthesis: (a) Photographs of large-scale $CsPbBr_3$ dispersion under normal indoor light. Inset provides the photograph of NC dispersion under UV illumination (355 nm excitation wavelength). (b) XRD pattern, (c) optical absorption (red line) and PL spectrum (black line), and (d) time-resolved PL of the large-scale $CsPbBr_3$ NCs with a 375 nm pulsed laser at room temperature (t=7.76 ns). Inset in panel b) reports the TEM image of the large-scale $CsPbBr_3$ NCs.

## Conclusions

A facile one-pot synthetic strategy to produce all-inorganic colloidal $CsPbX_3$ (X=Cl, Br, I, or mixed Cl/Br and Br/I) NCs with finely-tunable phases/compositions, morphologies, and optical properties has been developed. The evolution from perovskite $CsPbBr_3$ NPLs to nanosheets was accomplished by replacing OM with OTA as the capping ligand. The synthetic approach was extended from single halide NCs to mixed halide systems; using a combination of single/mixed halide NCs of varying controlled sizes, absorption spectra and PL emission bands can be finely-tuned over almost the entire visible spectral region (~411 to 694 nm). This general and facile synthetic route was conducted in open air, not requiring any vacuum process or inert gas protection. Scalable production of ink-like NC dispersion at atmospheric environment offers an opportunity for the deposition of $CsPbX_3$ NCs at large scale with high throughput and provides a potential cost advantage over conventional fabrication process. The compelling combination of scalability and reproducibility renders the present one-pot procedure appealing synthetic route for other perovskite NCs, which could accelerate the scale-up solution process for optoelectronic devices such as photovoltaics (PVs), quantum dot light-emitting diode (QLED), lasers and display applications.

## Conflicts of interest

There are no conflicts to declare.

## Acknowledgements

This work is supported by the National Undergraduate Innovation Program (No.20171049701020), the National Natural Science Foundation of China (No. 51461135004), Doctoral Fund of Ministry of Education Priority Development Project (No. 20130143130002) and Scientific Leadership Training Program of Hubei ([2012]86). We thank Dr. Chunhua Shen and Dr. Zhao Deng (Center of Materials Research and Testing, Wuhan University of Technology) for help with XRD and TEM/HRTEM characterization, respectively. We also thank Dr. Qi Zhang and Mr. Zhi Zheng (State Key Laboratory of Material and Processing and Die & Mould Technology, School of Materials Science and Engineering, Huazhong University of Science and Technology) for help with the test and analyses of PLQY. We would also like to thank Dr. Adam Clancy (University College of London, London WC1E 7JE, United Kingdom) for proofreading the manuscript.

### Notes and references

1. Q. A. Akkerman, V. D'Innocenzo, S. Accornero, A. Scarpellini, A. Petrozza, M. Prato and L. Manna, *J. Am. Chem. Soc.*, 2015, **137**, 10276-10281.
2. Q. A. Akkerman, S. G. Motti, A. R. Srimath Kandada, E. Mosconi, V. D'Innocenzo, G. Bertoni, S. Marras, B. A. Kamino, L. Miranda, F. De Angelis, A. Petrozza, M. Prato and L. Manna, *J. Am. Chem. Soc.*, 2016, **138**, 1010-1016.
3. R. Begum, M. R. Parida, A. L. Abdelhady, B. Murali, N. M. Alyami, G. H. Ahmed, M. N. Hedhili, O. M. Bakr and O. F. Mohammed, *J. Am. Chem. Soc.*, 2017, **139**, 731-737.
4. S. Dastidar, D. A. Egger, L. Z. Tan, S. B. Cromer, A. D. Dillon, S. Liu, L. Kronik, A. M. Rappe and A. T. Fafarman, *Nano Lett.*, 2016, **16**, 3563-3570.
5. J. De Roo, M. Ibáñez, P. Geiregat, G. Nedelcu, W. Walravens, J. Maes, J. C. Martins, I. Van Driessche, M. V. Kovalenko and Z. Hens, *ACS Nano*, 2016, **10**, 2071-2081.
6. C. de Weerd, L. Gomez, H. Zhang, W. J. Buma, G. Nedelcu, M. V. Kovalenko and T. Gregorkiewicz, *J. Phys. Chem. C*, 2016, **120**, 13310-13315.
7. I. Dursun, C. Shen, M. R. Parida, J. Pan, S. P. Sarmah, D. Priante, N. Alyami, J. Liu, M. I. Saidaminov, M. S. Alias, A. L. Abdelhady, T. K. Ng, O. F. Mohammed, B. S. Ooi and O. M. Bakr, *ACS Photonics*, 2016, **3**, 1150-1156.
8. Y. Fu, H. Zhu, C. C. Stoumpos, Q. Ding, J. Wang, M. G. Kanatzidis, X. Zhu and S. Jin, *ACS Nano*, 2016, **10**, 7963-7972.
9. C. Guhrenz, A. Benad, C. Ziegler, D. Haubold, N. Gaponik and A. Eychmüller, *Chem. Mater.*, 2016, **28**, 9033-9040.
10. J. B. Hoffman, A. L. Schleper and P. V. Kamat, *J. Am. Chem. Soc.*, 2016, **138**, 8603-8611.
11. H. Huang, B. Chen, Z. Wang, T. F. Hung, A. S. Susha, H. Zhong and A. L. Rogach, *Chem. Sci.*, 2016, **7**, 5699-5703.

12. T. C. Jellicoe, J. M. Richter, H. F. J. Glass, M. Tabachnyk, R. Brady, S. E. Dutton, A. Rao, R. H. Friend, D. Credgington, N. C. Greenham and M. L. Böhm, *J. Am. Chem. Soc.*, 2016, **138**, 2941-2944.
13. Y. Kim, E. Yassitepe, O. Voznyy, R. Comin, G. Walters, X. Gong, P. Kanjanaboos, A. F. Nogueira and E. H. Sargent, *ACS Appl. Mater. Interfaces*, 2015, **7**, 25007-25013.
14. B. A. Koscher, N. D. Bronstein, J. H. Olshansky, Y. Bekenstein and A. P. Alivisatos, *J. Am. Chem. Soc.*, 2016, **138**, 12065-12068.
15. X. Li, Y. Wu, S. Zhang, B. Cai, Y. Gu, J. Song and H. Zeng, *Adv. Funct. Mater.*, 2016, **26**, 2435-2445.
16. W. Liu, Q. Lin, H. Li, K. Wu, I. Robel, J. M. Pietryga and V. I. Klimov, *J. Am. Chem. Soc.*, 2016, **138**, 14954-14961.
17. F. Palazon, F. Di Stasio, Q. A. Akkerman, R. Krahne, M. Prato and L. Manna, *Chem. Mater.*, 2016, **28**, 2902-2906.
18. S. Pathak, N. Sakai, F. Wisnivesky Rocca Rivarola, S. D. Stranks, J. Liu, G. E. Eperon, C. Ducati, K. Wojciechowski, J. T. Griffiths, A. A. Haghighirad, A. Pellaroque, R. H. Friend and H. J. Snaith, *Chem. Mater.*, 2015, **27**, 8066-8075.
19. J. M. Pietryga, Y.-S. Park, J. Lim, A. F. Fidler, W. K. Bae, S. Brovelli and V. I. Klimov, *Chem. Rev.*, 2016, **116**, 10513-10622.
20. M. I. Saidaminov, A. L. Abdelhady, B. Murali, E. Alarousu, V. M. Burlakov, W. Peng, I. Dursun, L. Wang, Y. He, G. Maculan, A. Goriely, T. Wu, O. F. Mohammed and O. M. Bakr, *Nat. Commun.*, 2015, **6**, 7586.
21. X. Zhang, W. Cao, W. Wang, B. Xu, S. Liu, H. Dai, S. Chen, K. Wang and X. W. Sun, *NANO ENERGY*, 2016, **30**, 511-516.
22. J. Chen, L. Gan, F. Zhuge, H. Li, J. Song, H. Zeng and T. Zhai, *Angew. Chem. Int. Ed.* , 2017, **56**, 2390-2394.
23. P. Gao, M. Gratzel and M. K. Nazeeruddin, *Energ. Environ. Sci.*, 2014, **7**, 2448-2463.
24. Q. Pan, H. Hu, Y. Zou, M. Chen, L. Wu, D. Yang, X. Yuan, J. Fan, B. Sun and Q. Zhang, *J. Mater. Chem. C*, 2017, DOI: 10.1039/C7TC03774K.
25. S. Bai, Z. Yuan and F. Gao, *J. Mater. Chem. C*, 2016, **4**, 3898-3904.
26. Y. Bekenstein, B. A. Koscher, S. W. Eaton, P. Yang and A. P. Alivisatos, *J. Am. Chem. Soc.*, 2015, **137**, 16008-16011.
27. D. N. Dirin, L. Protesescu, D. Trummer, I. V. Kochetygov, S. Yakunin, F. Krumeich, N. P. Stadie and M. V. Kovalenko, *Nano Lett.*, 2016, **16**, 5866-5874.
28. J. Shamsi, Z. Dang, P. Bianchini, C. Canale, F. D. Stasio, R. Brescia, M. Prato and L. Manna, *J. Am. Chem. Soc.*, 2016, **138**, 7240-7243.
29. Q. A. Akkerman, M. Gandini, F. Di Stasio, P. Rastogi, F. Palazon, G. Bertoni, J. M. Ball, M. Prato, A. Petrozza and L. Manna, *Nat. Energy*, 2016, **2**, 16194.
30. Y. Zhao and K. Zhu, *Chem. Soc. Rev.*, 2016, **45**, 655-689.
31. Y. Wang, X. Li, X. Zhao, L. Xiao, H. Zeng and H. Sun, *Nano Lett.*, 2016, **16**, 448-453.
32. P. Ramasamy, D.-H. Lim, B. Kim, S.-H. Lee, M.-S. Lee and J.-S. Lee, *Chem. Commun.*, 2016, **52**, 2067-2070.
33. V. K. Ravi, G. B. Markad and A. Nag, *ACS Energy Lett.*, 2016, **1**, 665-671.
34. B. Luo, Y.-C. Pu, Y. Yang, S. A. Lindley, G. Abdelmageed, H. Ashry, Y. Li, X. Li and J. Z. Zhang, *J. Phys. Chem. C*, 2015, **119**, 26672-26682.
35. M. C. Weidman, M. Seitz, S. D. Stranks and W. A. Tisdale, *ACS Nano*, 2016, **10**, 7830-7839.
36. G. Nedelcu, L. Protesescu, S. Yakunin, M. I. Bodnarchuk, M. J. Grotevent and M. V. Kovalenko, *Nano Lett.*, 2015, **15**, 5635-5640.
37. J. A. Sichert, Y. Tong, N. Mutz, M. Vollmer, S. Fischer, K. Z. Milowska, R. García Cortadella, B. Nickel, C. Cardenas-Daw, J. K. Stolarczyk, A. S. Urban and J. Feldmann, *Nano Lett.*, 2015, **15**, 6521-6527.
38. I. Levchuk, P. Herre, M. Brandl, A. Osvet, R. Hock, W. Peukert, P. Schweizer, E. Spiecker, M. Batentschuk and C. J. Brabec, *Chem. Commun.*, 2017, **53**, 244-247.
39. P. Tyagi, S. M. Arveson and W. A. Tisdale, *J. Phys. Chem. Lett.*, 2015, **6**, 1911-1916.
40. D. Zhang, Y. Yu, Y. Bekenstein, A. B. Wong, A. P. Alivisatos and P. Yang, *J. Am. Chem. Soc.*, 2016, **138**, 13155-13158.
41. D. Zhang, Y. Yang, Y. Bekenstein, Y. Yu, N. A. Gibson, A. B. Wong, S. W. Eaton, N. Kornienko, Q. Kong, M. Lai, A. P. Alivisatos, S. R. Leone and P. Yang, *J. Am. Chem. Soc.*, 2016, **138**, 7236-7239.
42. D. Amgar, A. Stern, D. Rotem, D. Porath and L. Etgar, *Nano Lett.*, 2017, **17**, 1007-1013.
43. S. Sun, D. Yuan, Y. Xu, A. Wang and Z. Deng, *ACS Nano*, 2016, **10**, 3648-3657.
44. Z. Liang, S. Zhao, Z. Xu, B. Qiao, P. Song, D. Gao and X. Xu, *ACS Appl. Mater. Interfaces*, 2016, **8**, 28824-28830.
45. D. Zhang, S. W. Eaton, Y. Yu, L. Dou and P. Yang, *J. Am. Chem. Soc*, 2015, **137**, 9230-9233.
46. M. Imran, F. Di Stasio, Z. Dang, C. Canale, A. H. Khan, J. Shamsi, R. Brescia, M. Prato and L. Manna, *Chem. Mater.*, 2016, **28**, 6450-6454.
47. X. Chen, H. Hu, Z. Xia, W. Gao, W. Gou, Y. Qu and Y. Ma, *J. Mater. Chem. C*, 2017, **5**, 309-313.
48. L. Protesescu, S. Yakunin, M. I. Bodnarchuk, F. Krieg, R. Caputo, C. H. Hendon, R. X. Yang, A. Walsh and M. V. Kovalenko, *Nano Lett.*, 2015, **15**, 3692-3696.
49. A. Pan, B. He, X. Fan, Z. Liu, J. J. Urban, A. P. Alivisatos, L. He and Y. Liu, *ACS Nano*, 2016, **10**, 7943-7954.
50. L. Protesescu, S. Yakunin, M. I. Bodnarchuk, F. Krieg, R. Caputo, C. H. Hendon, R. X. Yang, A. Walsh and M. V. Kovalenko, *Nano Lett.*, 2015, **15**, 3692-3696.
51. A. Swarnkar, R. Chulliyil, V. K. Ravi, M. Irfanullah, A. Chowdhury and A. Nag, *Angew. Chem. Int. Ed*, 2015, **127**, 15644-15648.
52. X. Chen, L. Peng, K. Huang, Z. Shi, R. Xie and W. Yang, *Nano Res.*, 2016, **9**, 1994-2006.
53. E. Dilena, Y. Xie, R. Brescia, M. Prato, L. Maserati, R. Krahne, A. Paolella, G. Bertoni, M. Povia, I. Moreels and L. Manna, *Chem. Mater.*, 2013, **25**, 3180-3187.
54. Y. Xie, W. Chen, G. Bertoni, I. Kriegel, M. Xiong, N. Li, M. Prato, A. Riedinger, A. Sathya and L. Manna, *Chem. Mater.*, 2017, **29**, 1716-1723.
55. S. Wei, Y. Yang, X. Kang, L. Wang, L. Huang and D. Pan, *Chem. Commun.*, 2016, **52**, 7265-7268.
56. S. K. Balakrishnan and P. V. Kamat, *ACS Energy Lett.*, 2017, **2**, 88-93.
57. X. Zhang, H. Lin, H. Huang, C. Reckmeier, Y. Zhang, W. C. H. Choy and A. L. Rogach, *Nano Lett.*, 2016, **16**, 1415-1420.
58. J. Cho, Y.-H. Choi, T. E. O'Loughlin, L. De Jesus and S. Banerjee, *Chem. Mater.*, 2016, **28**, 6909-6916.
59. J. van Embden, A. S. R. Chesman and J. J. Jasieniak, *Chem. Mater.*, 2015, **27**, 2246-2285.

60. Y. Yu, D. Zhang, C. Kisielowski, L. Dou, N. Kornienko, Y. Bekenstein, A. B. Wong, A. P. Alivisatos and P. Yang, *Nano Lett.*, 2016, **16**, 7530-7535.
61. Z. Dang, J. Shamsi, F. Palazon, M. Imran, Q. A. Akkerman, S. Park, G. Bertoni, M. Prato, R. Brescia and L. Manna, *ACS Nano*, 2017, **11**, 2124-2132.

 